Sulphate Removal Induces a Major Conformational Change in Leishmania mexicana Pyruvate Kinase in the Crystalline State

ARTICLE *in* JOURNAL OF MOLECULAR BIOLOGY · SEPTEMBER 2008

Impact Factor: 4.33 · DOI: 10.1016/j.jmb.2008.08.037 · Source: PubMed

6 AUTHORS, INCLUDING:

Lindsay B Tulloch
University of St Andrews
19 PUBLICATIONS **283** CITATIONS
SEE PROFILE

Véronique Hannaert
Université catholique de Louvain
51 PUBLICATIONS **1,984** CITATIONS
SEE PROFILE

Paul Michels
The University of Edinburgh
231 PUBLICATIONS **9,918** CITATIONS
SEE PROFILE

Linda A Fothergill-Gilmore
The University of Edinburgh
131 PUBLICATIONS **3,356** CITATIONS
SEE PROFILE

doi:10.1016/j.jmb.2008.08.037 *J. Mol. Biol.* (2008) **383**, 615–626

JMB

Available online at www.sciencedirect.com

ScienceDirect

ELSEVIER

Sulphate Removal Induces a Major Conformational Change in *Leishmania mexicana* Pyruvate Kinase in the Crystalline State

Lindsay B. Tulloch[1], Hugh P. Morgan[1], Véronique Hannaert[2], Paul A. M. Michels[2], Linda A. Fothergill-Gilmore[1] and Malcolm D. Walkinshaw[1]*

[1]*Structural Biochemistry Group, Institute of Structural and Molecular Biology, The University of Edinburgh, Michael Swann Building, The King's Buildings, Mayfield Road, Edinburgh EH9 3JR, UK*

[2]*Research Unit for Tropical Diseases, de Duve Institute and Laboratory of Biochemistry, Université catholique de Louvain, Avenue Hippocrate 74, B-1200 Brussels, Belgium*

Received 11 August 2008; accepted 14 August 2008
Available online
23 August 2008

Edited by M. Guss

We report X-ray structures of pyruvate kinase from *Leishmania mexicana* (*Lm*PYK) that are trapped in different conformations. These, together with the previously reported structure of *Lm*PYK in its inactive (T-state) conformation, allow comparisons of three different conformers of the same species of pyruvate kinase (PYK). Four new site point mutants showing the effects of side-chain alteration at subunit interfaces are also enzymatically characterised. The *Lm*PYK tetramer crystals grown with ammonium sulphate as precipitant adopt an active-like conformation, with sulphate ions at the active and effector sites. The sulphates occupy positions similar to those of the phosphates of ligands bound to active (R-state) and constitutively active (nonallosteric) PYKs from several species, and provide insight into the structural roles of the phosphates of the substrates and effectors. Crystal soaking in sulphate-free buffers was found to induce major conformational changes in the tetramer. In particular, the unwinding of the Aα6′ helix and the inward hinge movement of the B domain are coupled with a significant widening (4 Å) of the tetramer caused by lateral movement of the C domains. The two new *Lm*PYK structures and the activity studies of site point mutations described in this article are consistent with a developing picture of allosteric activity in which localised changes in protein flexibility govern the distribution of conformer families adopted by the tetramer in its active and inactive states.

Keywords: conformational transitions; *Leishmania mexicana*; pyruvate kinase; X-ray crystallography

Introduction

Pyruvate kinase (PYK) catalyses the final reaction of glycolysis in which phosphoenolpyruvate (PEP) and ADP are converted into pyruvate and ATP, respectively. The enzyme is a homotetramer (Fig. 1a) composed of identical monomers of 50–60 kDa, depending on species. In mammals, the M1 (adult) isoenzyme is normally unregulated, whilst the M2 (embryonic and tumour), R (erythrocyte), and L (liver) isoenzymes are allosterically activated by fructose 1,6-bisphosphate (F-1,6-BP) and other effectors. Many PYKs from other species are also activated by F-1,6-BP, but trypanosomatid (*Trypanosoma* and *Leishmania*) PYKs are allosterically activated primarily by fructose 2,6-bisphosphate (F-2,6-

*Corresponding author. E-mail address: m.walkinshaw@ed.ac.uk.

Present address: L. B. Tulloch, Division of Biological Chemistry and Molecular Microbiology, School of Life Sciences, The Wellcome Trust Biocentre, The University of Dundee, Dow Street, Dundee DD1 5EH, UK.

Abbreviations used: *Lm*PYK, pyruvate kinase from *Leishmania mexicana*; PYK, pyruvate kinase; PEP, phosphoenolpyruvate; F-1,6-BP, fructose 1,6-bisphosphate; F-2,6-BP, fructose 2,6-bisphosphate; FBP, fructose bisphosphate; rM1PYK, rabbit M1 PYK; *Lm*PYK Glu451Trp, Glu451Trp mutant of *Lm*PYK; AS, ammonium sulphate; PG, phosphoglycollate; PDB, Protein Data Bank; TEA, triethanolamine.

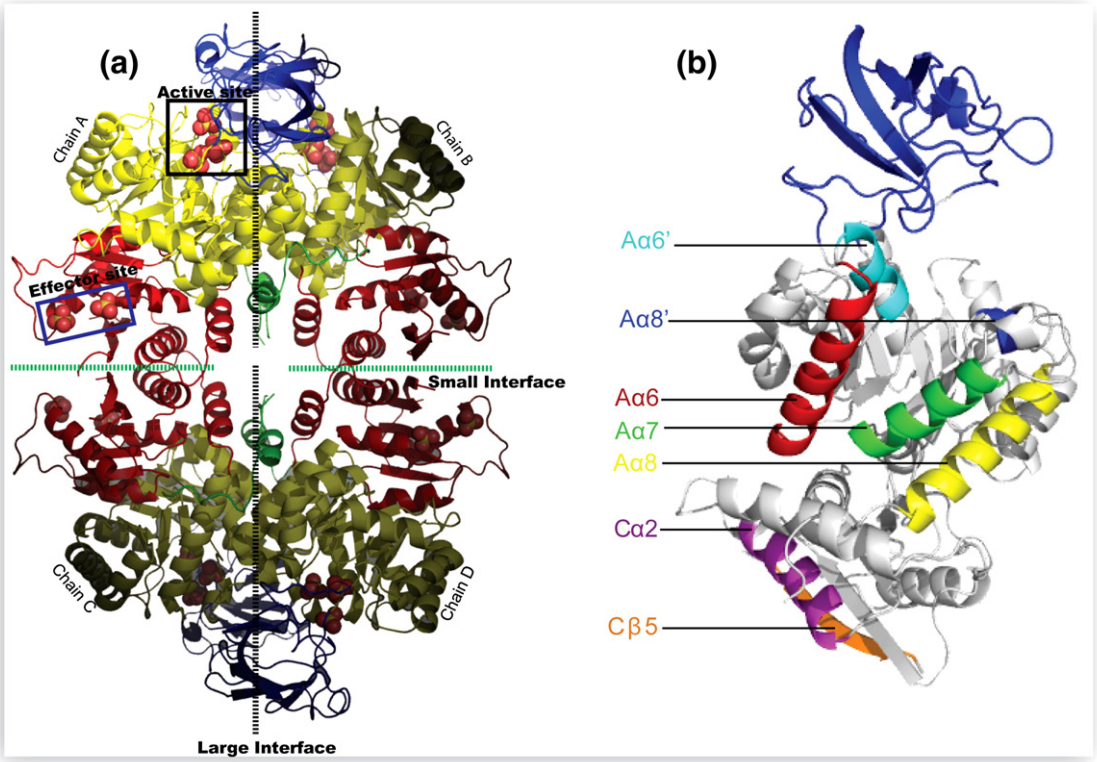

Fig. 1. Structure of sulphate-bound *Lm*PYK Glu451Trp showing domain boundaries and tetramer architecture. (a) The sulphate-bound *Lm*PYK Glu451Trp tetramer highlighting the active and effector sites. Chain A is shown in tones lighter than those of chains B, C, and D. Each monomer has been coloured to aid the identification of domains; N-terminal (green, residues 1–17), A (yellow, residues 18–88 and 187–356), B (blue, residues 89–186), and C (red, residues 358–498). The large (A–A) and small (C–C) interfaces between monomers are shown as dashed lines. (b) Chain A of sulphate-bound *Lm*PYK Glu451Trp. The B domain is shown in blue. Selected helices and strands are identified in the A and C domains.

BP), although they also respond to much higher (millimolar instead of micromolar) concentrations of F-1,6-BP.[1] A new regulatory mechanism has been discovered in the tumourigenic M2 isoform of PYK,[2] which releases its F-1,6-BP effector upon binding of specific phosphotyrosine peptides.[3]

Structures of PYK from seven species (with pairwise sequence identities as low as 41%) have now been solved in complex with various ligands (Table 1).[3–17] PYK monomers are composed of four domains: N-terminal, A, B, and C domains (Fig. 1). The N-terminal domain displays the most variation among PYKs, and while it is relatively long in erythrocyte and liver PYKs (84 and 53 amino acids, respectively), it is completely absent from prokaryote PYKs. This domain can be removed from human erythrocyte PYK with no effect on its stability or activity.[13] The A domain is an $(\alpha/\beta)_8$ barrel (comprising Aα1–Aα8 α helices and Aβ1–Aβ8 β strands) that forms the central core of the monomer and two additional helices, Aα6′ and Aα8′ (Fig. 1b). The Aα6, Aα7, and Aα8 helices of the $(\alpha/\beta)_8$ barrel constitute the A–A or 'large' interface between adjacent monomers (Fig. 1a). The B domain forms a mobile cap at one end of the $(\alpha/\beta)_8$-barrelled A domain, and the active site lies in the cavity between them. Comparisons of the active sites of inactive (T-state) PYK[10,11] with those of active (R-state) PYK[5,6,13] and constitutively active (M1) PYK[4,7] show that the inactive state generally has an open conformation that becomes partially closed through a hinge-type movement of the B domain upon enzyme activation. It is only when both substrates have bound that the active site closes fully around them[7] to allow the conversion of PEP and ADP into pyruvate and ATP, respectively. The C domain houses the effector site (Fig. 1a), which is located about 40 Å from the active site. Adjacent Cα2 helices and Cβ5 strands of the C domains form the C–C or 'small' interface between monomers (Fig. 1a), which is held together through reciprocal hydrogen bonds.

The allosteric conformational switch that transforms the tetramer to the active state may be achieved either through the binding of effector molecule [fructose bisphosphate (FBP)] or through the cooperative binding of PEP itself. Despite a wealth of structural data (Table 1), the fine details of the structural transition between the active state and the inactive state are not fully understood. Site-directed mutagenesis has been used extensively to identify residues that regulate allostery in PYK. Enzymatic measurements from a set of 14 site point mutants of yeast (*Saccharomyces cerevisiae*) PYK,[18] along with a study of rabbit M1 PYK (rM1PYK),[19] identified Glu392 in yeast PYK [corresponding to Lys421 in rM1PYK and to Glu390 in pyruvate kinase

Table 1. Crystal structures of PYK

Species	PDB code	Resolution	Active site ligands	Effector	State	Reference
L. mexicana	1PKL	2.35	None	SO_4	Inactive	Rigden *et al.*[11]
L. mexicana	3E0V	3.3	SO_4	SO_4	Sulphate-bound	This work
L. mexicana	3E0W	3.1	None	None	Sulphate-removed	This work
E. coli	1PKY	2.5	None	None	Inactive	Mattevi *et al.*[10]
E. coli R292D	1E0T	1.8	None	SO_4	Inactive	Valentini *et al.*[12]
E. coli R271L	1E0U	2	None	SO_4	Inactive	Valentini *et al.*[12]
Geobacillus stearothermophilus	2E28	2.4	None	SO_4	Inactive	Suzuli *et al.*[15]
Saccharomyces cerevisiae	1A3W	3	K^+, Mn^{2+}, PG	F-1,6-BP	Active	Jurica *et al.*[6]
S. cerevisiae	1A3X	3	K^+, Mn^{2+}, PG	None	Active	Jurica *et al.*[6]
Human erythrocyte	2VBG	2.73	K^+, Mn^{2+}, PG	F-1,6-BP	Active	Valentini *et al.*[13]
Human erythrocyte T384M	2VGF	2.75	K^+, Mn^{2+}, PG	F-1,6-BP	Active	Valentini *et al.*[13]
Human erythrocyte R479H	2VGG	2.74	K^+, Mn^{2+}, PG	F-1,6-BP	Active	Valentini *et al.*[13]
Human erythrocyte R486W	2VGI	2.87	K^+, Mn^{2+}, PG	F-1,6-BP	Active	Valentini *et al.*[13]
Cat (M1)	1PYK	2.6	None	None	Constitutively active	Stuart *et al.*[16]
Cat (M1)	1PKM	2.6	None	None	Constitutively active	Allen and Muirhead[4]
Rabbit (M1)	1PKN	2.9	K^+, Mn^{2+}, pyruvate	None	Constitutively active	Larsen *et al.*[9]
Rabbit (M1)	1F3W	3	K^+, Mn^{2+}, pyruvate	None	Constitutively active	Wooll *et al.*[17]
Rabbit (M1) S402P	1F3X	2.8	K^+, Mn^{2+}, pyruvate	None	Constitutively active	Wooll *et al.*[17]
Rabbit (M1)	1AQF	2.7	K^+, Mg^{2+}, phospholactate	None	Constitutively active	Larsen *et al.*[8]
Rabbit (M1)	1A49	2.1	K^+, Mg^{2+}, oxalate, ATP	None	Constitutively active	Larsen *et al.*[7]
Rabbit (M1)	1A5U	2.35	Na^+, Mg^{2+}, oxalate, ATP	None	Constitutively active	Larsen *et al.*[7]
Rabbit (M1)	2G50	1.65	Na^+, Mn^{2+}, pyruvate	Alanine	Inactive	Williams *et al.*[14]
Human (M2)	1ZJH	2.2	None	None	Inactive	Unpublished
Human (M2)	1T5A	2.8	K^+, Mg^{2+}, oxalate, PO_4	None	Active	Dombrauckas *et al.*[5]
Human (M2)	3BJT	2.5	Mg^{2+}, oxalate	None	Active	Christofk *et al.*[3]
Human (M2)	3BJF	2.03	K^+, Mg^{2+}, oxalate	F-1,6-BP	Active	Christofk *et al.*[3]

from *Leishmania mexicana* (*Lm*PYK)] as a key allosteric residue. Based on these mutagenesis results, a putative communication pathway between the effector site and the active site was hypothesised. An alternative mechanism based upon a comparison of the structure of inactive T-state *Escherichia coli* PYK[10] with the structure of the constitutively active rM1PYK[9] has also been described. Differences between these structures were used to suggest that an allosteric signal was transmitted via rotations of rigid domains of PYK.[20] Further structural and enzymatic characterisation studies of eight site point mutations located along the domain interfaces of *E. coli*PYK[10,12] showed the importance of domain interfaces in allosteric transition. The X-ray structure determination of human erythrocyte PYK and a study of eight mutants were carried out by the same group,[13] allowing a correlation of mutant properties with clinical symptoms. Although the effects of mutations were unpredictable, the work supported the idea that 'the T and R forms of PYK correspond to ensembles of conformers characterised by the flexibility of the B domain.'[17] This idea has been developed, and there is now some experimental evidence to show that ligand binding can differentially affect the dynamics of domains and that allosteric regulation of PYK may be determined by the distribution of an ensemble of states in which T and R represent the two extremes.[21] This allosteric model is consistent with many of the published site-directed mutagenesis studies on PYK reported here and previously,[22–24] which show that single mutations distant from the effector and active sites can have unpredictably profound effects on the rates of enzyme catalysis. Of potential medical interest are the 122 naturally occurring mutations that have been identified in human erythrocyte PYK and are linked to the disease nonspherocytic haemolytic anemia.[25] A number of these mutations, occurring mainly in the C domain, are not highly conserved over the 241 species and isoforms examined and are therefore hypothesised to play a role in allostery.

The two new structures of PYK from *L. mexicana* described here show different conformational states. A sulphate-bound conformer with sulphate ions at the active and effector sites has a partially closed active site resembling that of an active conformer of PYK.[8] A 'sulphate-removed' conformer displays conformational changes throughout the tetramer caused by a change in the water hydrogen-bonding network and the loss of a key sulphate bridge between the A domain and the B domain. These new structures provide further evidence that PYK is a conformationally dynamic molecule that can exist as a conformer intermediate between the extremes of a fully inactive T-state and a fully active R-state, and may provide insight into the relationship between allosteric regulation and protein dynamics.[26–28]

Results and Discussion

Properties of the Glu451Trp mutant of *Lm*PYK

Tryptophan fluorescence quenching studies have previously been used to identify effectors of yeast PYK whereby the change in the environment of its single tryptophan residue, exposed near the surface of the effector site, was monitored through the quenching of its fluorescence.[29] *Lm*PYK does not contain any tryptophan residues, so one was introduced by site-directed mutagenesis in the

Table 2. Kinetic properties of wild-type and mutant *Lm*PYK

Ligand	Effector	Kinetic parameter	*Lm*PYK construct					
			Wild type[a]	S314N	S314Q	D315N	D315S	E451W
ADP[b]		K_m (mM)	0.214±0.021	ND	ND	ND	ND	0.371±0.03
		n	1.0					1.0
PEP[c]	None	$S_{0.5}$ (mM)	1.06±0.06	5.11±0.271	0.457±0.021	2.80±0.116	3.66±0.852	1.30±0.073
		n	1.55±0.14	1.50±0.103	1.68±0.121	1.97±0.131	1.09±0.112	1.69±0.12
		V_{max} (%)[d]	100[d]	69	48	3.7	1.4	72
	F-2,6-BP	$S_{0.5}$ (mM)	0.165±0.012	0.496±0.022	0.207±0.016	1.51±0.046	2.27±0.298	0.216±0.026
		n	1.26±0.069	1.91±1.12	1.48±1.04	1.67±0.518	1.72±2.07	1.53±0.13
F-2,6-BP[e]		$S_{0.5}$ (μM)	0.082±0.008	0.403±0.077	0.122±0.025	1.00±0.138	1.61±0.121	0.177±0.008
		n	1.0	1.0	1.0	1.0	1.0	1.0

ND, not determined.
[a] Where assays were performed at different times, they were performed against wild-type *Lm*PYK controls. All data have been normalised to those of a control experiment.
[b] When [ADP] was varied, [PEP] was kept constant at 5 mM.
[c] When [PEP] was varied, [ADP] was kept constant at 2 mM. Assays conducted in the absence or in the presence of 10 μM F-2,6-BP.
[d] These values are expressed relative to the wild-type enzyme; a typical value was 134 U/mg.
[e] When [F-2,6-BP] was varied, [PEP] and [ADP] were kept constant at 0.7 and 0.3 mM, respectively.

position corresponding to tryptophan in yeast PYK (Glu451Trp) to enable convenient screening for effector site ligands. This mutant was expressed in *E. coli* at high levels and was also used for the crystallographic studies reported here. The kinetic properties of the Glu451Trp mutant of *Lm*PYK (*Lm*PYK Glu451Trp) do not differ significantly from those of the wild-type enzyme (Table 2).

Sulphate-bound *Lm*PYK crystallised from ammonium sulphate has a partially closed active site

Crystals of *Lm*PYK Glu451Trp were grown in the presence of 16% (saturated) ammonium sulphate (AS). Improved X-ray resolution was obtained by soaking these crystals in a 40% (saturated) AS solution (Table 3). The refined structure contains sulphate ions at the active and effector sites (Fig. 2a and b); none of the other ligands present in the hanging-drop [including phosphoglycollate (PG) and F-1,6-BP] could be identified in the final refined crystal structure. The asymmetric unit contains six monomers: chains A–D form a complete tetramer, while chains E and F form a tetramer with their symmetry partners by means a crystallographic 2-fold axis. Despite the relatively modest resolution of the X-ray data (3.3 Å), the side chains are well defined, and the six monomers of the asymmetric unit are all very similar, with average RMSD of 0.04 Å for C^{α} atoms of residues 1–498.

The sulphate-bound tetramer of *Lm*PYK Glu451Trp was superimposed onto *Lm*PYK1PKL (the crystal structure of the 'inactive T-form' of *Lm*PYK crystallised in polyethylene glycol[11]). The RMS fit of the 1532 C^{α} atoms of the A and C domains (residues 10–89 and 190–498) using all four tetramer chains is only 0.8 Å, indicating no major conformational or structural differences between the tetramers for these two domains. There is, however, a large movement of the B domain towards the A domain in the sulphate-bound structure compared with *Lm*PYK1PKL (Fig. 2a–c). The program DynDom[30] was used to analyse this movement, which shows that the B domain pivots around prolines 87 and 187 and rotates towards the A domain by 33.5° (Table 4), resulting in partial closure of the active site (Figs. 2 and 3a, b, d). Structures of the human tumour M2 PYK crystallised with F-1,6-BP and oxalate [Protein Data Bank (PDB) code 1T5A; Table 1] and with no ligand (1ZJH; Table 1), showing that the B domain rotates towards the A domain by 20° in the ligand-bound structure, were also analysed. Four structures of rM1PYK containing different ligands are also available (Table 1), and a DynDom analysis of 2G50 (containing pyruvate in the active site and alanine in the allosteric amino acid binding site) with 1A49 (with ATP and oxalate in the active site) shows the B domain rotated towards the A domain by 26° in the rM1PYK 1A49 structure (Table 4).

Sulphate ions mimic the phosphates of PEP and ATP in the active site

Three highly conserved sulphate ions are bound at identical positions in the active sites of all six monomers of the asymmetric unit and have peak heights greater than 6σ in an unbiased $F_o - F_c$ map (Fig. 2a and b). The sulphate ion interacting with Arg49, Asn51, and Lys238 (the γ-sulphate; Fig. 2a and c) occupies the same position as the γ-phosphate of ATP in the constitutively active rabbit muscle enzyme structure in complex with oxalate and ATP (1A49; Table 1). The same site is occupied by the phosphate of the PEP analogue PG in the active-state structures of yeast[6] and human erythrocyte[5] PYKs.

A second sulphate ion (the β-sulphate; Fig. 2a and c) interacts with His54 from the A domain and with Arg175 from domain B, forming a bridge between the A domain and the B domain (Figs. 2c and 3e) and locking the active site in a partially closed state. This β-sulphate mimics the β-phosphate of ATP, which

Table 3. *Lm*PYK crystal statistics

Crystal form	Crystal form 1[a] (SO_4 bound)	Crystal form 2[b] (SO_4 removed)
Crystallisation conditions		
Precipitant	AS 16% saturated	AS 15% saturated
Buffer	0.1 M Na citrate (pH 4.6)	0.1 M Na citrate (pH 4.4)
Ligands in mother liquor	10 mM PG and 25 mM F-1,6-BP	10 mM PG and 25 mM F-1,6-BP
Ligands in crystal	SO_4^{2-}	None
Soaking solution	AS 40% (sat), 0.1 M Na citrate (pH 4.6), 10 mM PG, and 25 mM F-1,6-BP	NaCl 45% (sat) and 0.1 M Na citrate (pH 4.4)
Crystal statistics		
Space group	$P\,4_2\,2_1\,2$	$P\,4_2\,3\,2$
Unit cell dimensions		
a, *b*, *c* (Å)	261.95, 261.95, 185.54	185.55, 185.55, 185.55
α, β, γ (°)	90.00, 90.00, 90.00	90.00, 90.00, 90.00
Solvent content (%)	73.4	73.0
Scaling statistics		
Data collection location	SRS 9.6	SRS 14.2
Resolution range		
Overall (Å)	99.01–3.3	40.26–3.1
Outer shell (Å)	3.48–3.3	3.27–3.1
Number of measurements	264,216	159,620
Unique reflections	86,237	19,992
Redundancy	3.1 (2.7)[c]	10.2 (9.1)[c]
Completeness	89.4 (89.4)[c]	99.5 (99.5)[c]
$\langle I/\sigma(I)\rangle$	8.9 (1.6)[c]	11.8 (1.5)[c]
R_{merge}	7.5 (49.6)[c]	4.1 (37.5)[c]
Wilson *B* ($Å^2$)	98.1	108.4
Refinement statistics		
R_{work} (%)/number of reflections	22.7/80,266	21.5/18,969
R_{free} (%) /number of reflections	29.0/5971	24.7/1023
RMSD bond length (Å)	0.009	0.006
RMSD bond angle (°)	1.244	1.053
Ramachandran		
Core region (%)	87.9	87.4
Allowed region (%)	11.5	11.4
Generously allowed region (%)	0.5	1.2
Model statistics		
Subunits per asymmetric unit	6	1
Protein residues		
Total (number/average *B*-factor)	2970/48.0	485/102.8
Number in of subunits A–F	494 497 494 495 495 495	485
B-factor of subunits A–F	74.6 74.6 74.4 74.6 75.3 74.8	102.8
Additional groups		
Solvent (No. number/average *B*-factor)	314/56.875 / 90.7	75/90.7
SO_4^{2-} 501 (*B*-factor, subunits A–F)	100.2 103.4 105.9 105.4 99.7 102.5	—
SO_4^{2-} 502 (*B*-factor, subunits A–F)	78.4 83.6 83.1 81.6 87.8 84.7	—
SO_4^{2-} 503 (*B*-factor, subunits A–F)	123.8 140.6 125.7 136.8 152.3 147.3	—
SO_4^{2-} 504 (*B*-factor, subunits A–F)	124.0 — 129.0 — 113.0 —	—
SO_4^{2-} 505 (*B*-factor, subunits A–F)	— 141.4 138.1 151.7 — —	—
SO_4^{2-} 506 (*B*-factor, subunits A–F)	111.2 72.6 103.3 105.5 118.0 101.8	—
SO_4^{2-} 507 (*B*-factor, subunits A–F)	78.6 85.0 78.6 69.0 78.9 79.0	—
SO_4^{2-} 508 (*B*-factor, subunits A–F)	130.4 147.7 143.3 — — 153.9	—

[a] Crystal soaked in 40% (saturated) AS.
[b] Sulphates removed by soaking crystals in 45% (saturated) NaCl.
[c] Values in parentheses are those for the highest-resolution shell.

binds to the corresponding residues (His77 and Arg119 in rabbit M1 numbering) in the rM1PYK complex (1A49; Table 1).[7]

The two sulphate ions in the effector site mimic the phosphates of F-2,6-BP

The effector sites of four of the monomers of *Lm*PYK Glu451Trp (A,B, C, and F) are complexed with two sulphates [S(i) and S(ii) Fig. 2b and d], whilst two monomers (D and E) contain only one sulphate. The sulphate common to all six monomers, S(i), is bound in the same position as the 6-phosphate of F-1,6-BP in yeast,[6] human erythrocyte,[13] and tumour[5] PYKs. The second sulphate, S(ii), is found in four monomers in the crystal and sits in a pocket formed by Arg456, Asn401, His480, and Lys453 (Fig. 2d). This is the position close (~1 Å) to phosphate-1 of F-1,6-BP in the crystal structures of yeast,[6] human erythrocyte,[13] and tumour[5] PYKs.

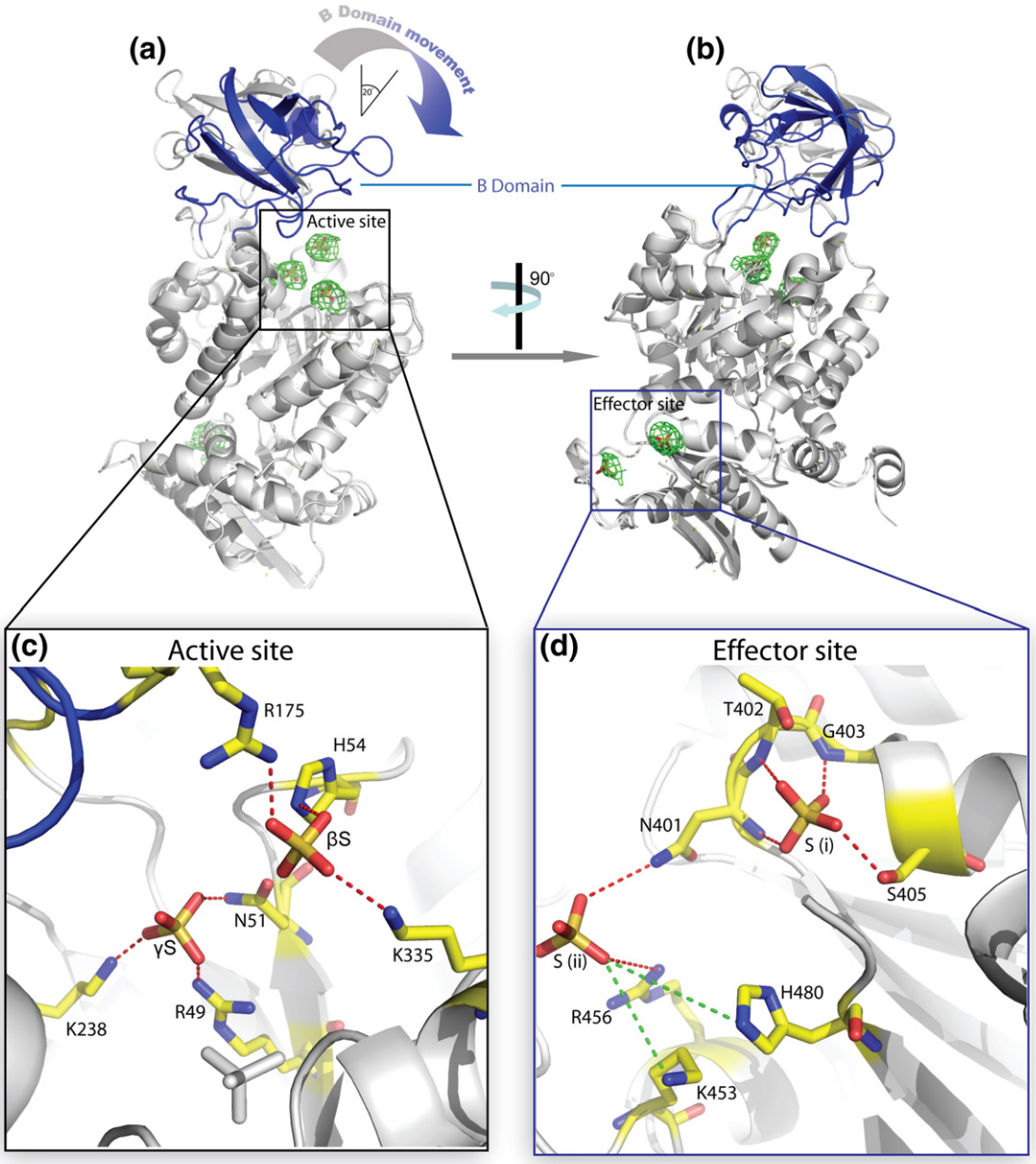

Fig. 2. Comparison of the sulphate-bound form of *Lm*PYK Glu451Trp and the 'inactive' form of *Lm*PYK1PKL showing sulphate ions in the active and effector sites. All sulphate ions are shown as sticks, and conserved hydrogen bonds are shown as red dashed lines. Hydrogen bonds not conserved in all chains are shown as green dashed lines. (a and b) Two orthogonal views of chain A of *Lm*PYK Glu451Trp complexed with sulphate superimposed onto the 'inactive' *Lm*PYK1PKL structure. The RMS fit of the C^{α} atoms of domains A and C (residues 18–86 and 188–480) is 0.2 Å. The B domain (residues 87–187) is shown in blue for the sulphate-bound *Lm*PYK Glu451Trp structure. The 33° movement of domain B corresponding to the closure of the active site is highlighted. The sulphate positions are shown by an unbiased $F_o - F_c$ electron density map (green) contoured at 3σ. (c) The active site sulphate ion γS occupies a position close to the γ-phosphate of ATP (in structure 1A49). This site is occupied by the phosphate of PG in yeast PYK (1A3X) and human erythrocyte PYK (1LIU). The βS sulphate ion mimics the β-phosphate of ATP in structure 1A49. It forms hydrogen bonds with His54 and Lys335 from the A domain and with Arg175 from the B domain, making a bridge between the A domain and the B domain. (d) The effector site/sulphate ions mimic the phosphates of F-2,6-BP. Sulphate ion S(i) is found in all six chains and is bound in the same position as the 6-phosphate of F-1,6-BP in yeast (1A3W), human erythrocyte (1LIU), and tumour (1T5A) PYKs. The second sulphate, S(ii), is found in four monomers in the crystal and sits in a position close to the phosphate-1 of F-1,6-BP in the same crystal structures of yeast, human erythrocyte, and tumour PYKs.

Modelling studies suggest that, although the sulphates in the *Lm*PYK structure are positioned in the expected phosphate positions, the furanose ring of F-1,6-BP/F-2,6-BP would clash with the flexible loop (residues His480-Gln491) and Cβ4 strand. The flexible loop and Cβ4 strand are therefore likely to move during F-1,6-BP/F-2,6-BP binding, possibly affecting the geometry of the small interface.

Table 4. DynDom analysis

Source	Confomer 1	Confomer 2	Moving domain	Bending residues	Rotation angle (°)	Closure (%)	RMSD of A, C, and N-terminal domains (Å)
L. mexicana	1PKL (T)[a]	SO_4	89–186	86–90, 186–190	33.5	57.3	0.5
L. mexicana	1PKL (T)	SO_4_Free	88–186	87–89, 184–187	37.0	58.8	1.57
Human tumour (M2)	1ZJH (T)[a]	1TGA (R)[a]	115–220	114–117, 219–221	20.3	98.1	0.98
Rabbit muscle (M1)	2G50 (T)[a]	1A49 (R)[a]	118–216	116–118, 216–222	26.3	88.9	0.43

T, tight (inactive) state; R, relaxed (active) state.
[a] Please see Table 1 for references.

Sulphate removal by crystal soaking induces changes in tetramer shape

The structure of *Lm*PYK Glu451Trp crystallised from AS in the presence of FBP and PG showed that sulphate ions were apparently able to outcompete these two ligands, as no PG or FBP was found in the structure. In order to make a sulphate-free form for ligand soaking experiments, crystals were back-soaked in 45% (saturated) NaCl. This had a dramatic effect on tetramer shape and structure, with crystals changing from a tetragonal space group with six chains in the asymmetric unit to a cubic space group with one chain in the asymmetric unit (Table 3).

The sulphate-free cubic form of *Lm*PYK, which was refined using data up to 3.1 Å, forms a tetramer with exact crystallographic D_2 symmetry. Interestingly, this sulphate-free tetramer is significantly less tightly packed than the sulphate-bound form, although the crystal packing in both the cubic form and the tetragonal form shows large solvent channels with very similar values for the Matthews coefficient corresponding to 73% hydration.

As a measure of the packing density in the tetramer, all interchain nonbonded contacts were calculated. In the sulphate-bound form, each chain makes between 160 and 168 interatomic contacts of $\leq$3.7 Å with adjacent chains in the tetramer and involves 59 amino acids. (As the D_2 symmetry of the sulphate-bound tetramer is noncrystallographic, the number of contacts is not identical for each chain.) This compares with only 85 nonbonded contacts of $\leq$3.7 Å from 33 amino acids from each chain of the sulphate-free cubic form (showing exact crystallographic D_2 symmetry). The weakening of interchain contact is more dramatic at the large interface (residues Met1-Pro14, Ala270-Ala288, Arg310-Asn321, and Pro339-Gln356), where contacts drop from about 90 (involving 29 amino acids) down to only 27 (involving 15 residues) in the sulphate-removed tetramer. The contacts in the small interface (Pro373-Thr391 and Ala482-Val495) are better conserved, with some 70 contacts (from 20 residues) in the sulphate-bound structure compared with 57 contacts (from 18 residues) in the sulphate-free structure.

A least squares fit of the C^{α} atoms of domains A and C (residues 10–89 and 190–498) onto the corresponding atoms of the sulphate-bound structure gave an RMS fit of 2.1 Å (Fig. 3c and f). The comparison shows that (when viewed as in Fig. 1a, with the long axis of the tetramer vertical) the removal of the sulphates results in a vertical collapse of the B domain towards the A domain by about 2 Å. There is also a significant movement of the A domain along the (α/β) barrel axis (indicated by arrows in Fig. 3f), which has the effect of moving apart adjacent A domains, consistent with the weaker and presumably less constrained A–A (large) interface of the sulphate-free form.

In concert with movements of the A and B domains, there is an outward horizontal movement of each of the C domains by an average of about 2 Å (Fig. 3f). For example, the twofold related Glu454 C^{α} atoms sitting at the end of helix Cα5 are separated by 88 Å in the sulphate-free form compared with 83 Å in the sulphate-bound form (Fig. 3b and c). This essentially translational movement of the C domains has little effect on the contacts between the C domains over the C–C interface. These 'small interface' contacts seem to be better preserved because the C domains of the twofold related chains forming the interface move in the same direction, whereas the compression of the tetramer that results from crystal soaking and sulphate removal causes the A domains forming the large interface to be pushed apart. The net result of these concerted domain movements caused by crystal soaking and sulphate removal is that the tetramer adopts a squat shape, which is over 4 Å wider than the sulphate-bound form (Fig. 3c and f).

The Aα6′ helix and N-terminal helices unwind in the sulphate-free structure

The crystal soaking treatment performed to remove sulphate that causes the domain and interchain slippage described above also has an effect on secondary structures: both the two-turn N-terminal helix (Ser2-Ser10) and the short Aα6′ helix (R262-E267) are unwound in the sulphate-free form. The N-terminal helix found in the sulphate-bound structure and in *Lm*PYK1PLK contributes significantly to the large interface of the tetramer. Each of the four short 12-residue N-terminal domains makes an average of 13 van der Waals contacts to the neighbouring chain across the 'large interface.' The two N-termini from the dimer chains forming one

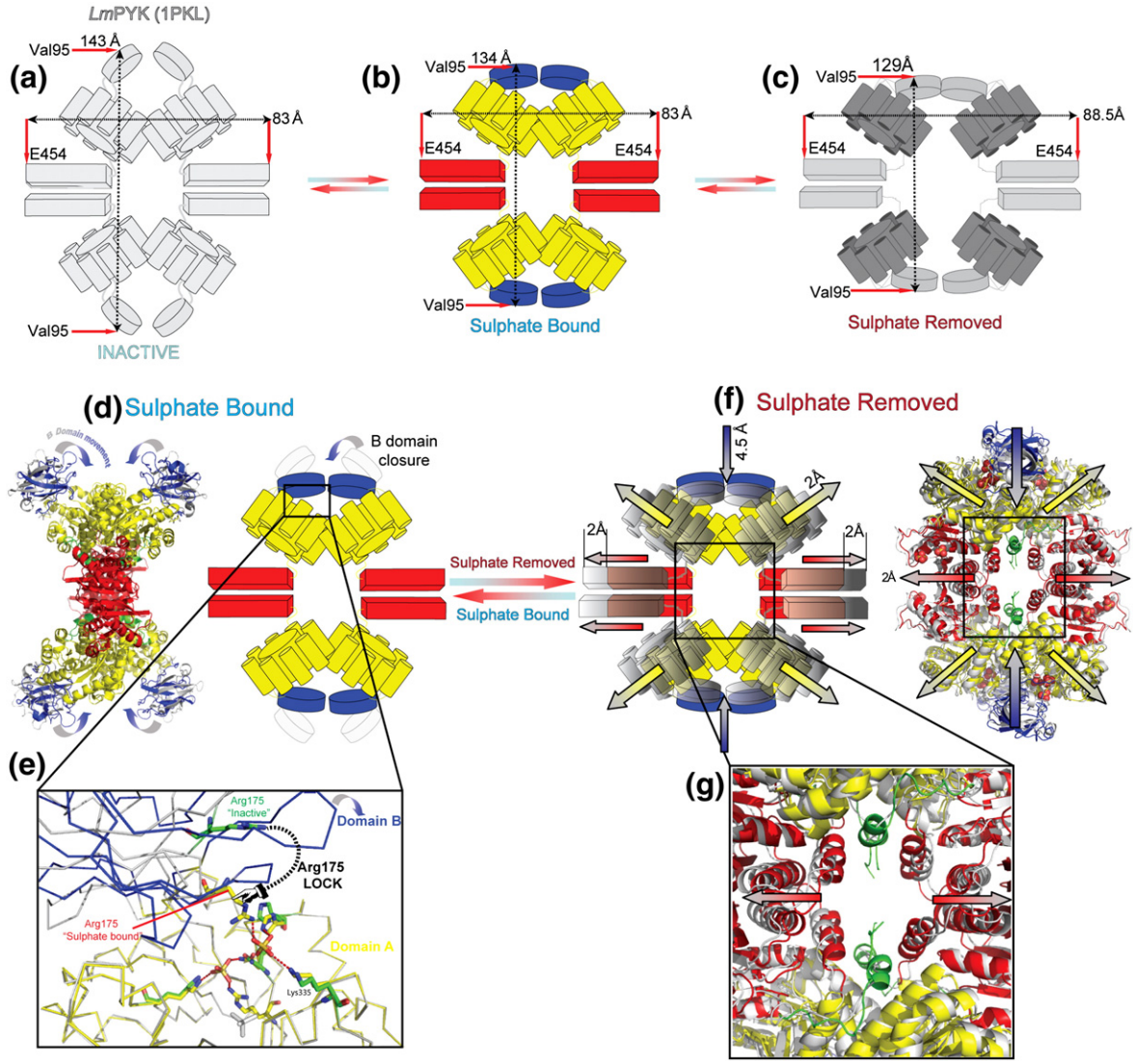

Fig. 3. Comparisons of three *Lm*PYK structures ('inactive' *Lm*PYK1PKL and the sulphate-bound and sulphate-removed forms of *Lm*PYK Glu451Trp) showing domain and chain movements. (a) Schematic representation of the structure of the 'inactive' *Lm*PYK1PKL tetramer structure showing selected distances that help define the tetramer dimensions. The distance between Glu454(C^{α}) chain A and the corresponding atom in chain B across the large interface is 83 Å. The distance between Val95(C^{β}) chain A and the corresponding atom in chain C across the small interface is 143 Å. (b) Schematic representation of the structure of the sulphate-bound *Lm*PYK Glu451Trp tetramer structure. The domains have been coloured as follows: B, blue; A, yellow; C, red. The distances as in (a) show an identical width (83 Å). The movement of the B domain shortens the tetramer by 9 Å. (c) Schematic representation of the structure of the sulphate-removed *Lm*PYK Glu451Trp tetramer structure showing the same selected distances as in (a) and (b). Compared with (b), the overall dimensions of the tetramer decrease in length by about 5 Å as the B domain closes down into the A domain, and there is widening of the tetramer by about 4 Å as the C domains move laterally. (d) Schematic representation of *Lm*PYK1PKL (a) overlaid on the sulphate-bound form of *Lm*PYK (b). The A and C domains superpose well in the tetramer with an RMS fit of C^{α} atoms of less than 1 Å, highlighting the difference in the orientations of the B domains. (e) An enlargement of the active site area from the sulphate-bound structure (coloured as in Fig. 1a) superimposed onto the inactive *Lm*PYK structure (1PKL; in gray). Residues involved in sulphate binding are shown as sticks (carbon atoms are shown in yellow for the *Lm*PYK Glu451Trp structure and in green for the 1PKL structure), and a dashed line has been added to show the movement of Arg175 between the two *Lm*PYK forms. The Arg175 locks the B domain in a partially closed conformation (Fig. 2c). (f) An overlay of (b) and (c): the sulphate-bound and the sulphate-free structures. Arrows show the direction of domain movements after crystal soaking and sulphate removal. The RMS fit of C^{α} atoms from residues 18–86 and 188–480 for all four chains was 2.1 Å. (g) An enlargement of the core of the *Lm*PYK tetramer showing the movement of C domains between the sulphate-bound *Lm*PYK structure and the sulphate-free structure (gray).

'large interface' in the tetramer (e.g., the interface between chains A and B in Fig. 1a) contribute independently to the large interface. Thus, for the sulphate-bound structure with a total of 90 van der Waals contacts, 26 are contributed from the N-terminal domain.

Removal of the β-sulphate from the ADP-binding pocket of the active site (Fig. 2c) results in loss of the sulphate bridge between the A domain and the B domain, and thereby allows the B domain to fold towards the A domain with a concomitant unwinding of helix Aα6′ (Fig. 4). It is noteworthy that the short two-turn Aα6′ helix (^{262}RGDLGVE^{267}) contains two glycine residues (usually regarded as helix breakers) that are also conserved in yeast, rabbit, human, and *E. coli* sequences. In the sulphate-bound structure, the N-terminus of the Aα6′ helix is capped and stabilised by a hydrogen bond between the amide nitrogen of Gly263 and the side chain of Thr296. The adjacent residue Gln297 forms a hydrogen bond with Arg310, which sits at the end of the Aα7 helix of a neighbouring chain (Fig. 4). Another interchain hydrogen bond between Arg310 and the carbonyl of Gly263 is observed in most published PYK structures (Table 1). The unwinding of the short unstable Aα6′ helix results in significant (~2 Å) movements of the helices at the 'large interface,' loss of the Thr296-Gly263 hydrogen bond, and repositioning of the side chains of Arg310 and Gln297 (Fig. 4). The importance of the cross-interface interaction of Arg310 has been demonstrated in previous mutagenesis studies,[12,13] where mutation of the residue always results in loss of activity.

Site point mutations at the 'large interface' affect enzymatic activity

The two conformational states found in the sulphate-bound and sulphate-free forms show that the 'large interface' can be tightly fitted with many nonbonded contacts or can be pushed apart (in the sulphate-free form), with the interface held together by relatively few interactions. We present site-directed mutagenesis results to examine the role of this interface in catalytic activity (Table 2).

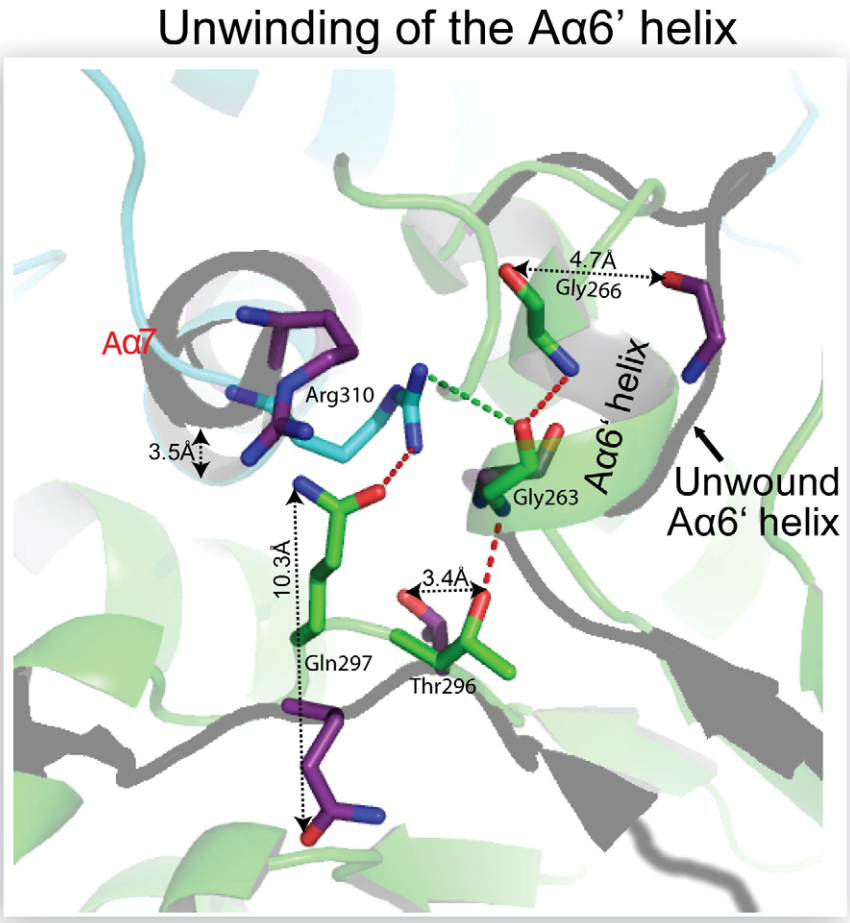

Fig. 4. Unwinding of the short Aα6′ helix on crystal soaking and sulphate removal. A section of the A–A interface for the sulphate-bound form of *Lm*PYK (chain A is shown in green, and chain B is shown in blue) overlaid with the same region from the sulphate-removed structure (in gray with purple side chains). In the sulphate-bound form, the two-turn helix is stabilised by hydrogen bond interactions Arg310…Gly263 and Thr296…Gly263. In the sulphate-free crystal, residues Arg262-Glu267 now adopt a coil conformation, and all hydrogen bonds stabilising the helix have been broken. Movements of amino acids are illustrated using a double-headed arrow. Conserved hydrogen bonds are shown as red dashed lines, and frequently observed hydrogen bonds are shown as green dashed lines. There is a pronounced movement of helix Aα7 by over 3 Å.

The central interaction of the large interface of inactive PYK is formed by Ser314 and Asp315 (located in the middle of the Aα7 helix), which hydrogen bond to Asp315 and Ser314, respectively, on the neighbouring chain. This twofold related interaction is disrupted in the sulphate-free structure. Both residues were mutated in attempts to stabilise or disrupt the interaction. A Ser314Gln mutation induced a partial activation of the enzyme, increasing the affinity of the mutant PYK for PEP, suggesting that destabilisation of the central interaction of the large interface (characterised by a more flexible tetramer) favours substrate binding. Conversely, Ser314Asn, Asp315Asn, and Asp315Ser mutations each appeared to stabilise the interaction at the large interface, preventing monomer rotations and reducing affinity for PEP. Indeed, communication between active sites is almost completely lost in the Asp315Ser mutant, which displays an almost hyperbolic response to PEP in the absence of effector. It can also be seen that mutations of Asp315 are accompanied by a substantial decrease in V_{max}.

Interestingly, the Asp315Ser, Asp315Asn, and, to a lesser extent, Ser314Asn mutations cause up to a 20-fold reduced affinity for F-2,6-BP binding to the effector site and also significantly lower V_{max} values (Table 2), suggesting that these remote changes affecting tetramer flexibility have an effect on the effector binding pocket and on the transmission of the allosteric signal.

PYK may have a dynamic mechanism of activation

The site point mutation data presented here for *Lm*PYK and for a number of other PYKs[25] show that profound changes in enzymatic activity can be achieved by a broad variety of mutants remote from the active site or the effector site. In the above example, mutations in the large interface are some 30 Å away from the binding site where the effects are observed.

Recent analyses suggest that enzyme mechanisms involve a dynamic sampling of families of conformational substrates.[31] An extension of this idea is that the change in the flexibility of regions of a protein caused by allosteric effects, defined as any change in the state of the protein caused by ligand binding,[32] could play an important role in regulating enzyme or allosteric activity.[33] The two *Lm*PYK structures presented here suggest that the sulphate (ligand)-bound structure is less flexible than the (wider) sulphate-free form (in which the A6′ helix is melted and there are fewer 'large interface' contacts). The two tetramer forms have rather different overall shapes, with the tall, thin sulphate-bound form being converted into the short, fat form by concerted movements of the A, B, and C domains in different relative directions. Such a picture is consistent with the suggestion that differences in the flexibility (dynamic properties) of PYK, as modulated by ligand binding or site point mutations, could play a major role in relaying the allosteric signal.

Materials and Methods

Cloning and site-directed mutagenesis

The *L. mexicana* PYK mutants Glu451Trp, Ser314Gln, Ser314Asn, Asp315Asn, and Asp315Ser were constructed using PCR techniques previously described,[23] whilst the *Lm*PYK Asn178Ala mutant was created using the Stratagene QuickChange mutagenesis kit. DNA sequencing was used to confirm that the mutations had been incorporated into the sequences.

Protein expression and purification

Wild-type and mutant *Lm*PYKs were over expressed in *E. coli* BL21(DE3) cells using the pET28 vector[23] and carried an N-terminal extension of 20 residues including a $(His)_6$-tag. Cells were induced with 1 mM isopropyl-β-D-thiogalactopyranoside at 18 °C for 24 h and were harvested by centrifugation. Cells from 1 L of culture were resuspended in 20 ml of buffer S [50 mM triethanolamine (TEA)/HCl, 150 mM KCl, 0.5 mM K_2HPO_4, 2 mM NaN_3, and 20% (wt/vol) glycerol pH 7.2] supplemented with ethylenediaminetetraacetic-acid-free proteolytic inhibitor mini tablets (Roche), lysed with 10 mg/ml lysozyme, and sonicated. Nucleic acids were precipitated with protamine sulphate (200 mg/20 ml cell extract), and cell debris was removed by centrifugation. Cell extracts were stored at −20 °C or used immediately for protein purification.

His-tagged *Lm*PYKs were purified by TALON (BD Biosciences Clontech) (Co^{2+}) metal-affinity chromatography. Weakly bound peptides were eluted with buffer S supplemented with 10 mM imidazole, and pure *Lm*PYK was eluted with buffer S supplemented with 100 mM imidazole. Fractions were screened for PYK activity with saturating concentrations of substrates (2.5 mM PEP and 2 mM ADP) and pooled (see Protein Characterisation). Purity was assessed by Bradford assay[34] (Pierce's Coomassie Plus Reagent) and SDS-PAGE. [35] Pooled protein fractions were then stored in aliquots at −20 °C for protein characterisation or buffer-exchanged into 20 mM TEA/HCl (pH 7.2) using a disposable PD10 desalting column (GE Healthcare), concentrated to 10.5 mg/ml, and stored at −20 °C for crystallisation.

Protein characterisation

Assays for the comparison of wild-type and mutant *Lm*PYKs were conducted as described by Hannaert *et al.*[23] The assay buffer contained 50 mM TEA/HCl buffer (pH 7.2), 50 mM KCl, and 6 mM Mg_2SO_4. The kinetic parameters of PEP and ADP were determined in saturating conditions whereby [ADP] was constant at 2 mM when [PEP] was varied, and [PEP] was constant at 5 mM when [ADP] was varied. When [F-2,6-BP] was varied, substrates were subsaturated, whereby [PEP] was constant at 0.7 mM and [ADP] was constant at 0.3 mM.

Crystallisation

Crystals of *Lm*PYK Glu451Trp were grown using the hanging-drop method of vapour diffusion at 4 °C. Protein solutions comprised *Lm*PYK Glu451Trp at 7 mg/ml dissolved in 20 mM TEA buffer (pH 7.2), 10 mM $MgCl_2$, 200 mM KCl, 10 mM PG, and 25 mM F-1,6-BP. (F-1,6-BP

was used at 10-fold $S_{0.5}$ rather than F-2,6-BP because F-2,6-BP was less stable and was not commercially available.) Well solutions comprised 10–20% saturated AS and 100 mM sodium citrate/citric acid buffer (pH 4.0–4.6). Hanging drops consisted of 1.5 μl of protein solution and 1.5 μl of well solution. Crystals of tetragonal form 1 (Table 3) developed overnight and grew to maximum dimensions of 0.4 mm × 0.4 mm × 0.2 mm after 1 week. No attempt was made to remove the N-terminal His-tag extension prior to crystallisation. Crystals of poor morphology were also obtained in the absence of PG and F-1,6-BP, but failed to diffract X-rays.

Crystals of tetragonal form 1 (Table 3) diffracted poorly (to 3.8 Å), so crystals were dehydrated by soaking in 40% (saturated) AS, 100 mM sodium citrate/citric acid buffer, 10 mM $MgCl_2$, 200 mM KCl, 10 mM PG, and 25 mM F-1,6-BP. It is noteworthy that determination of the structures of unsoaked crystals also revealed sulphates at both active and effector sites.

To remove sulphate from the active and effector sites of the protein, unsoaked crystals of tetragonal form 1 were serially transferred to solutions containing decreasing concentrations of AS and increasing concentrations of NaCl, into a final solution of 45% saturated NaCl, 100 mM sodium citrate/citric acid buffer (pH 4.2), and 35% (wt/vol) glycerol. Crystals were soaked in the final soaking solutions for periods ranging from 2 h to 1 month and always adopted the cubic crystal form 2 (Table 3).

X-ray data collection

Sulphate-bound crystals of tetragonal crystal form 1 were immersed in cryoprotectant consisting of mother/soaking liquor supplemented with 35% (vol/vol) glycerol before flash freezing in liquid N_2. The soaking solution for sulphate-free crystals of cubic form 2 was suitable as a cryoprotectant, so sulphate-free crystals were flash frozen directly from the soaking solutions.

Data were collected at the SRS facility, Daresbury, UK, on beamlines 9.6, 14.1, and 14.2. For crystals of tetragonal form 1, the phi scans were 0.25° and 120°. For crystals of cubic form 2, the phi scans were 0.5° and 45°.

The CCP4 suite was used for the processing and refinement of X-ray data.[36] All data were indexed and integrated with MOSFILM[37] and scaled with SCALA.

Structure solution and refinement

For both tetragonal and cubic crystal forms, the initial phases were estimated by molecular replacement with MOLREP,[38] using the inactive-state wild-type *Lm*PYK (PDB entry 1PKL[11]) as search model. The sulphate-bound model was improved through 20 cycles of rigid-body refinement, followed by several rounds of tight NCS-restrained TLS refinement with REFMAC5.[39] NCS and TLS groups corresponded to the four domains of each monomer: NCS/TLS group 1 comprised residues 1–88 and 187–357 (N and A domains); NCS/TLS group 2 comprised residues 89–186 (B domain); and NCS/TLS group 3 comprised residues 358–498 (C domain). NCS restraints were loosened towards completion and completely removed for the final refinement. The sulphate-free structure was refined similarly, but NCS restraints were omitted as only one monomer was present in the asymmetric unit. Manual adjustments to the models were performed with Coot.[40] Three hundred and fourteen water molecules were added to the sulphate-bound model during rebuilding with Coot,[32] while 75 water molecules were added to the sulphate-free structure. Geometries of models were assessed using PROCHECK. Figures were generated with PyMOL.[41]

PDB accession codes

The atomic coordinates of *Lm*PYK Glu451Trp complexed with sulphate have been submitted to the PDB as entry 3E0V. The structure of *Lm*PYK Glu451Trp following sulphate removal has been submitted as entry 3E0W.

Acknowledgements

Thanks to Dr. Iain McNae for help with X-ray data collection and refinement, Dr. Jorge Iulek for help with model refinement, Dr. Daniel Rigden for suggesting suitable *Lm*PYK mutations, and Cédric Yernaux for help with construction of mutants. This study was supported by the European Commission under its INCO-DEV program (contract ICA4-CT-2001-10075) and the UK Medical Research Council.

References

1. Ernest, I., Callens, M., Opperdoes, F. R. & Michels, P.A. (1994). Pyruvate kinase of *Leishmania mexicana mexicana*. Cloning and analysis of the gene, overexpression in *Escherichia coli* and characterization of the enzyme. *Mol. Biochem. Parasitol.* **64**, 43–54.
2. Christofk, H. R., Vander Heiden, M. G., Harris, M. H., Ramanathan, A., Gerszten, R. E., Wei, R. *et al.* (2008). The M2 splice isoform of pyruvate kinase is important for cancer metabolism and tumour growth. *Nature*, **452**, 230–233.
3. Christofk, H. R., Vander Heiden, M. G., Wu, N., Asara, J. M. & Cantley, L. C. (2008). Pyruvate kinase M2 is a phosphotyrosine-binding protein. *Nature*, **452**, 181–186.
4. Allen, S. & Muirhead, H. (1996). Refined three-dimensional structure of cat-muscle (M1) pyruvate kinase at a resolution of 2.6 A. *Acta Crystallogr. Sect. D*, **52**, 499–504.
5. Dombrauckas, J. D., Santarsiero, B. D. & Mesecar, A. D. (2005). Structural basis for tumor pyruvate kinase M2 allosteric regulation and catalysis. *Biochemistry*, **44**, 9417–9429.
6. Jurica, M. S., Mesecar, A., Heath, P. J., Shi, W., Nowak, T. & Stoddard, B. L. (1998). The allosteric regulation of pyruvate kinase by fructose-1,6-bisphosphate. *Structure*, **6**, 195–210.
7. Larsen, T. M., Benning, M. M., Rayment, I. & Reed, G. H. (1998). Structure of the bis (Mg^{2})–ATP–oxalate complex of the rabbit muscle pyruvate kinase at 2.1 Å resolution: ATP binding over a barrel. *Biochemistry*, **37**, 6247–6255.
8. Larsen, T. M., Benning, M. M., Wesenberg, G. E., Rayment, I. & Reed, G. H. (1997). Ligand-induced domain movement in pyruvate kinase: structure of the enzyme from rabbit muscle with Mg^{2+}, K^{+}, and l-phospholactate at 2.7 Å resolution. *Arch. Biochem. Biophys.* **345**, 199–206.
9. Larsen, T. M., Laughlin, L. T., Holden, H. M., Rayment, I. & Reed, G. H. (1994). Structure of rabbit muscle pyruvate kinase complexed with Mn^{2+}, K^{+}, and pyruvate. *Biochemistry*, **33**, 6301–6309.

10. Mattevi, A., Valentini, G., Rizzi, M., Speranza, M. L., Bolognesi, M. & Coda, A. (1995). Crystal structure of *Escherichia coli* pyruvate kinase type I: molecular basis of the allosteric transition. *Structure*, **3**, 729–741.
11. Rigden, D. J., Phillips, S. E. V., Michels, P. A. M. & Fothergill-Gilmore, L. A. (1999). The structure of pyruvate kinase from *Leishmania mexicana* reveals details of the allosteric transition and unusual effector specificity. *J. Mol. Biol.* **291**, 615–635.
12. Valentini, G., Chiarelli, L., Fortin, R., Speranza, M. L., Galizzi, A. & Mattevi, A. (2000). The allosteric regulation of pyruvate kinase. *J. Biol. Chem.* **275**, 18145–18152.
13. Valentini, G., Chiarelli, L. R., Fortin, R., Dolzan, M., Galizzi, A., Abraham, D. J. *et al.* (2002). Structure and function of human erythrocyte pyruvate kinase. Molecular basis of nonspherocytic hemolytic anemia. *J. Biol. Chem.* **277**, 23807–23814.
14. Williams, R., Holyoak, T., McDonald, G., Gui, C. & Fenton, A. W. (2006). Differentiating a ligand's chemical requirements for allosteric interactions from those for protein binding. Phenylalanine inhibition of pyruvate kinase. *Biochemistry*, **45**, 5421–5429.
15. Suzuli, K., Ito, S., Shimizu-Ibuka, A. & Sakai, H. (2008). Crystal structure of pyruvate kinase from *Geobacillus stearothermophilus*. *J. Biochem.* **144**, 305–312.
16. Stuart, D. I., Levine, M., Muirhead, H. & Stammers, D. K. (1979). Crystal structure of cat muscle pyruvate kinase at a resolution of 2.6 Å. *J. Mol. Biol.* **134**, 109–142.
17. Wooll, J. O., Friesen, R. H. E., White, M. A., Watowich, S. J., Fox, R. O., Lee, J. C. & Czerwinski, E. W. (2001). Structural and functional linkages between subunit interfaces in mammalian pyruvate kinase. *J. Mol. Biol.* **312**, 525–540.
18. Fenton, A. W. & Blair, J. B. (2002). Kinetic and allosteric consequences of mutations in the subunit and domain interfaces and the allosteric site of yeast pyruvate kinase. *Arch. Biochem. Biophys.* **397**, 28–39.
19. Friesen, R. H. E., Castellani, R. J., Lee, J. C. & Braun, W. (1998). Allostery in rabbit pyruvate kinase: development of a strategy to elucidate the mechanism. *Biochemistry*, **37**, 15266–15276.
20. Mattevi, A., Bolognesi, M. & Valentini, G. (1996). The allosteric regulation of pyruvate kinase. *FEBS Lett.* **389**, 15–19.
21. Lee, J.C., Modulation of allostery of pyruvate kinase by shifting of an ensemble of microstates. *Acta Biochim. Biophys. Sin.* (Shanghai), **40**, 663-669.
22. Collins, R. A., Kelly, S. M., Price, N. C., Fothergill-Gilmore, L. A. & Muirhead, H. (1996). Ligand-induced conformational changes in wild-type and mutant yeast pyruvate kinase. *Protein Eng. Des. Sel.* **9**, 1203–1210.
23. Hannaert, V., Yernaux, C., Rigden, D. J., Fothergill-Gilmore, L. A., Opperdoes, F. R. & Michels, P. A. M. (2002). The putative effector-binding site of *Leishmania mexicana* pyruvate kinase studied by site-directed mutagenesis. *FEBS Lett.* **514**, 255–259.
24. Ikeda, Y., Tanaka, T. & Noguchi, T. (1997). Conversion of non-allosteric pyruvate kinase isozyme into an allosteric enzyme by a single amino acid substitution. *J. Biol. Chem.* **272**, 20495–20501.
25. Pendergrass, D. C., Williams, R., Blair, J. B. & Fenton, A. W. (2006). Mining for allosteric information: natural mutations and positional sequence conservation in pyruvate kinase. *IUBMB Life*, **58**, 31–38.
26. Hilser, V. J. & Thompson, E. B. (2007). Intrinsic disorder as a mechanism to optimize allosteric coupling in proteins. *Proc. Natl. Acad. Sci.* **104**, 8311.
27. Kern, D. & Zuiderweg, E. R. P. (2003). The role of dynamics in allosteric regulation. *Curr. Opin. Struct. Biol.* **13**, 748–757.
28. Yu, S., Lee, L. L. Y. & Ching Lee, J. (2003). Effects of metabolites on the structural dynamics of rabbit muscle pyruvate kinase. *Biophys. Chem.* **103**, 1–11.
29. Collins, R. A., McNally, T., Fothergill-Gilmore, L. A. & Muirhead, H. (1995). A subunit interface mutant of yeast pyruvate kinase requires the allosteric activator fructose 1,6-bisphosphate for activity. *Biochem. J.* **310**, 117.
30. Hayward, S. & Berendsen, H. J. C. (1998). Systematic analysis of domain motions in proteins from conformational change: new results on citrate synthase and T4 lysozyme. *Proteins*, **30**, 144–154.
31. Henzler-Wildman, K. A., Thai, V., Lei, M., Ott, M., Wolf-Watz, M., Fenn, T. *et al.* (2007). Intrinsic motions along an enzymatic reaction trajectory. *Nature*, **450**, 838–844.
32. Kuriyan, J. & Eisenberg, D. (2007). The origin of protein interactions and allostery in colocalization. *Nature* (London), **450**, 983.
33. Popovych, N., Sun, S., Ebright, R. H. & Kalodimos, C. G. (2006). Dynamically driven protein allostery. *Nat. Struct. Mol. Biol.* **13**, 831–838.
34. Bradford, M. M. (1976). A rapid and sensitive method for the quantitation of microgram quantities of protein utilizing the principle of protein–dye binding. *Anal. Biochem.* **72**, 248–254.
35. Laemmli, U. K. (1970). Cleavage of structural proteins during the assembly of the head of bacteriophage T4. *Nature*, **227**, 680–685.
36. Bailey, S. (1994). The CCP4 suite: programs for protein crystallography. *Acta Crystallogr. Sect. D*, **50**, 760–763.
37. Powell, H. R. (1999). The Rossmann Fourier autoindexing algorithm in MOSFLM. *Logo*, **55**, 1690–1695.
38. Lebedev, A. A., Vagin, A. A. & Murshudov, G. N. (2008). Model preparation in MOLREP and examples of model improvement using X-ray data. *Logo*, **64**, 33–39.
39. Murshudov, G. N., Vagin, A. A. & Dodson, E. J. (1997). Refinement of macromolecular structures by the maximum-likelihood method. *Acta Crystallogr. Sect. D*, **53**, 240–255.
40. Emsley, P. & Cowtan, K. (2004). Coot: model-building tools for molecular graphics. *Acta Crystallogr. Sect. D*, **60**, 2126–2132.
41. DeLano, W. L. (2002). *The PyMOL Molecular Graphics System.* DeLano Scientific, San Carlos, CA.